Tuning Nitrogen Species and Content in Carbon Materials through Constructing Variable Structures for Supercapacitors

SUN Peng[1,2], ZHANG Shaoning[1,3], BI Hui[1], DONG Wujie[1], HUANG Fuqiang[1,3,4]

(1. State Key Laboratory of High Performance Ceramics and Superfine Microstructure, Shanghai Institute of Ceramics, Chinese Academy of Sciences, Shanghai 200050, China; 2. Center of Materials Science and Optoelectronics Engineering, University of Chinese Academy of Sciences, Beijing 100049, China; 3. School of Physical Science and Technology, ShanghaiTech University, Shanghai 200031, China; 4. State Key Laboratory of Rare Earth Materials Chemistry and Applications, College of Chemistry and Molecular Engineering, Peking University, Beijing 100871, China.)

Abstract: Carbon materials are favorable for supercapacitors but suffer from insufficient capacitance. Heteroatom doping, especially nitrogen (N) doping, is an effective method to significantly improve the electrochemical performance, but it is still a big challenge to achieve high active nitrogen content in carbon materials. This work successfully tuned nitrogen species and content by interaction between Si–O–Si network and aluminum oxide. Besides, the structure of carbon materials varies from a coral-like network to three-dimensional structure by adjusting the precursor composition. Oxygen (O) in oxides bonds with N in carbon materials during the reaction, which makes it difficult to escape, achieving high nitrogen content of 5.29at% at 1000 ℃. On the other hand, the interaction empowers the carbon material with large pore volume of ~1.78 $cm^3 \cdot g^{-1}$ and broad pore size distribution of 0.5–60 nm. Thus, the N-rich carbon material harvests high capacitance of 302 $F \cdot g^{-1}$ at 1 $A \cdot g^{-1}$ and excellent rate capability of 177 $F \cdot g^{-1}$ at 120 $A \cdot g^{-1}$. This unique nitrogen fixation method is a promising strategy for preparing high performance electrode materials of supercapacitors.

Key words: carbon material; nitrogen fixation; interaction; morphology design; supercapacitor

Currently, carbon materials are the promising electrode materials in supercapacitors due to its outstanding electrical conductivity, high surface area, extraordinary electrochemical stability and low cost[1-3]. Nevertheless, the specific capacitance of commercial activated carbon is about 200 $F \cdot g^{-1}$, falling short of the practical applications[4]. Heteroatom doping (*e.g.*, N, P and S) is an efficient approach to improve the capacitance[5-6]. Among different N doping types, pyridinic nitrogen (N-6) and pyrrolic nitrogen (N-5) are effectively active sites, which can provide much pseudocapacitance. Hence, how to achieve high active nitrogen content in carbon materials is the key issue for next generation supercapacitors.

Two methods are proposed in recent works. One common way is to lower the pyrolysis temperature at the cost of conductivity loss[7-8]. Generally, low-temperature pyrolysis leads to high nitrogen content in the carbon materials, because the increasing sintering temperature enhances the graphitization degree, reduces the defects and edge sites. The other approach is to dope phosphorus to adjust the active N proportion but not total nitrogen content[9-10]. Previous work suggests that P-doping could result in high distortion of carbon structures, consequently producing defects and open edge sites in the N-doped carbon materials[10]. The defects and edge sites in the carbon materials play important roles in achieving a high proportion of pyridinic-N. Therefore, the construction of N-rich carbon materials with high electrical conductivity is extremely challenging.

Herein, we designed the N-rich carbon material by introducing both Si–O–Si network and aluminum oxide at 1000 ℃ for supercapacitors. The interaction between Si–O–Si network and aluminum oxide can promote the activity of oxygen atoms in oxides, making O in oxides

bond with N, main active N in carbon, which is beneficial for achieving high nitrogen content. Additionally, the Si–O–Si network and aluminum oxide as templates also empower the carbon material with large pore volume, 3D interconnected and hierarchical porous structure. Thus, these features lead to the excellent performance for supercapacitors with this N-rich carbon material.

1　Experimental

1.1　Sample preparation

1.1.1　Preparation of precursors

All reagents were of analytical grade and used without any purification. In a typical synthesis, 2 g of triblock copolymer polyethylene oxide-polypropylene oxide-polyethylene oxide (PEO-PPO-PEO) (P-123) as the surfactant, 1 mL of pyrrole as the nitrogen and carbon source, 3 g of $Al(NO_3)_3 \cdot 9H_2O$ or 4 mL of tetraethyl orthosilicate (TEOS) was added, respectively, or both $Al(NO_3)_3 \cdot 9H_2O$ and TEOS were added. Then, 0.4 mL of 1 $mol \cdot L^{-1}$ HCl and 50 μL of $FeCl_3$ (50 $mg \cdot mL^{-1}$) were continuously dissolved in 10.0 mL of ethanol. Finally, the solution was kept at 60 ℃ in oven overnight. For comparison, the gel without TEOS and $Al(NO_3)_3 \cdot 9H_2O$, was prepared by the above procedure.

1.1.2　Preparation of variable-structure carbon materials

The precursors were ground into powders, and heated under H_2 (20 sccm) and Ar (300 sccm) flows at 1000 ℃ (heating rate: 10 $℃ \cdot min^{-1}$) for 2 h. The furnace was cooled to 400 ℃ at 10 $℃ \cdot min^{-1}$ before natural cooling to the room temperature. The residual oxides were removed in a mixed solution of 6 $mol \cdot L^{-1}$ H_3PO_4 and 8 $mol \cdot L^{-1}$ HF to obtain the carbon materials. To improve electrochemical performance, N doping was promoted by providing NH_3 flow (100 sccm) in the heating process. The prepared carbon materials were denoted as NC (without the addition of $Al(NO_3)_3 \cdot 9H_2O$ and TEOS), AlO-NC (with the addition of $Al(NO_3)_3 \cdot 9H_2O$), SiO-NC (with the addition of TEOS), and SiAlO-NC (with the addition of both $Al(NO_3)_3 \cdot 9H_2O$ and TEOS), respectively.

1.2　Characterization

The microstructures were observed by an emission scanning electron microscope (SEM, Hitachi S-4800) and a transmission electron microscope (TEM, JEOL 2100F). Raman spectra were collected on a thermal dispersive spectrometer (λ=532 nm, 10 mW). X-ray diffraction (XRD) was performed on a Bruker D8 Advanced diffractometer with Cu-Kα irradiation (λ=0.15406 nm, 2θ=10°–80°). Specific surface areas and pore size distributions were obtained by nitrogen adsorption measurements, performed with ASAP 2020M (Micromeritics). X-ray photoelectron spectroscopy (XPS, Thermo VG Scientific) was carried out under vacuum using Al-Kα irradiation (1486.6 eV) generated at 400 W and 15 kV.

2　Results and discussion

Variable-structure carbon materials were prepared by tuning the compositions of precursors, as shown in Fig. 1. Firstly, self-assembly process of Pluronic P123 takes place[11]. Then, TEOS gradually hydrolyzes to form Si–O–Si network. In the sintering process, $Al(NO_3)_3 \cdot 9H_2O$ is dehydrated into aluminum oxide, and Al–N bonding forms in the NH_3 atmosphere. Meanwhile, Si–O–Si network interacts with Al–N bonding. On one hand, the interaction between Si–O–Si network and Al–N bonding introduces more defects and promotes O in oxides bond with N in carbon materials during the reaction, which makes it difficult to escape, achieving high nitrogen content. On the other hand, this empowers carbon materials with high pore volume and broad pore size distribution. The detailed discussion is provided below.

The addition of $Al(NO_3)_3 \cdot 9H_2O$ and TEOS affects the morphology and structures of as-prepared carbon materials. First, the morphology of these carbon materials varies by adjusting the precursor composition, which is coral-like for NC, sphere-like for AlO-NC and 3D for SiO-NC and SiAlO-NC in Fig. 2(a–d). The coral-like morphology for NC is attributed to the co-assembling between pyrrole and the surfactant template[11]. NC shows microporous structure in Fig. 2(e). After adding $Al(NO_3)_3 \cdot 9H_2O$ and lowering solution pH, self-assembling process of P123 is influenced. Therefore, pyrrole monomer polymerizes to sphere-like polypyrrole precursor, independently[12]. Then, after chemical vapor deposition
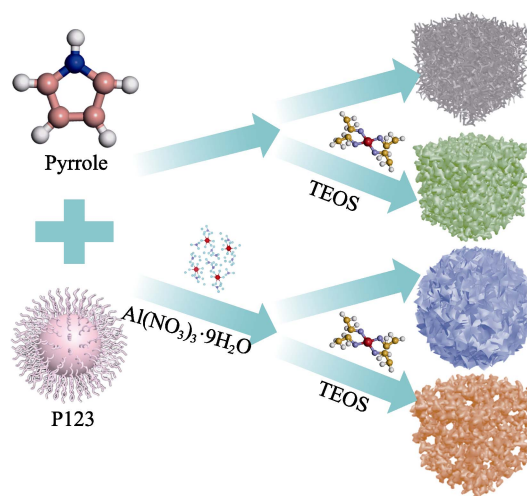

Fig. 1　Schematic processing route from precursors to variable-structure carbon materials
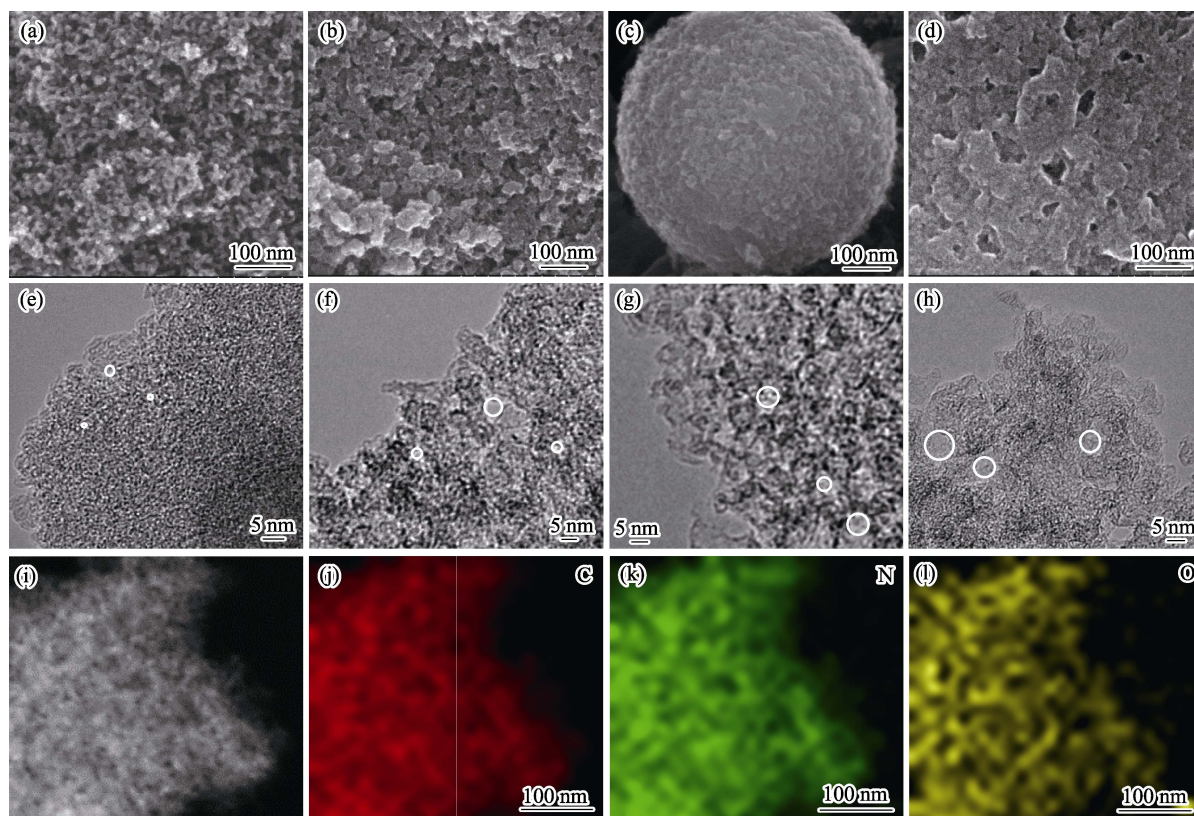
Fig. 2   (a–d) SEM and (e–h) HRTEM images of (a, e) NC, (b, f) SiO-NC, (c, g) AlO-NC and
(d, h) SiAlO-NC, and (i–l) energy dispersive spectroscopy (EDS) elemental mappings of SiAlO-NC

(CVD), the sphere-like carbon material, AlO-NC, with abundant mesopores is prepared in Fig. 2(f). The 3D skeletons of SiO-NC and SiAlO-NC are formed by Si–O–Si network and P123, separated by many disordered mesopores[13]. These structures are in accordance with what are observed in high-resolution TEM (HRTEM) (Fig. 2(g–h)). The corresponding elemental mappings of SiAlO-NC confirm homogeneous distributions of C, N and O elements in SiAlO-NC, as shown in Fig. 2(i–l).

Moreover, these carbon materials have diverse pore size distributions. With the interaction of oxides, the pore structure becomes richer. This phenomenon is demonstrated by the nitrogen adsorption-desorption isotherms (Fig. 3(a)) and pore size distributions (Fig. 3(b)). SiAlO-NC possesses the richest pore structure that distributes from 0.5 to 60 nm. As listed in Table 1, SiAlO-NC has large surface area (703.20 $m^2 \cdot g^{-1}$) and total pore volume (1.78 $cm^3 \cdot g^{-1}$) resulting from the interaction between the Si–O–Si network and $Al(NO_3)_3 \cdot 9H_2O$. Wide pore size distribution is beneficial for the rate capability of the material. However, all of the other materials display narrow distribution. In addition, Raman spectra reflect the difference (Fig. S1(a)). I_D/I_G is 1.00 for NC, 1.01 for SiO-NC, 1.03 for AlO-NC and 1.02 for SiAlO-NC. The D band at ~1340 cm^{-1} is commonly ascribed to the defects and edges of graphene-like carbon

materials, and the intensity ratio of D band to G band (~1570 cm^{-1}) typically suggests the defect degree of carbon materials[14].

Furthermore, the presence of oxides also increases the N contents of carbon materials even at high temperature (1000 ℃) (Table 1). From XPS spectra, nitrogen content of SiAlO-NC is 5.29at%, which is higher than those of NC (1.42at%), SiO-NC (1.66at%), and AlO-NC (3.52at%).

The phenomenon is rarely reported for N-doped carbon materials, tuning nitrogen content particularly at temperatures as high as 1000 ℃. For demonstrating the phenomenon, C1s and N1s XPS spectra of the carbon materials (Fig. 3(c–d) and Fig. S2) are deconvoluted. The C1s spectrum of SiAlO-NC is deconvoluted at 284.7, 285.3, 286.5, and 288.5 eV, corresponding to sp^2 C, N-bonded sp^2 C, N-bonded sp^3 C and C–O, respectively[15]. Its N1s band is deconvoluted at 398.5, 400.0, and 401.3 eV, corresponding to pyridinic nitrogen, pyrrolic nitrogen, and graphitic nitrogen, separately[16]. After etching, the atomic percentage of active nitrogen is 0.24% for NC, 0.58% for SiO-NC, 2.53% for AlO-NC and 3.70% for SiAlO-NC. SiAlO-NC owns the highest nitrogen and active nitrogen contents, which are attributed to the interaction between Si–O–Si network and aluminum oxide. This hypothesis can be demonstrated by the following analysis.
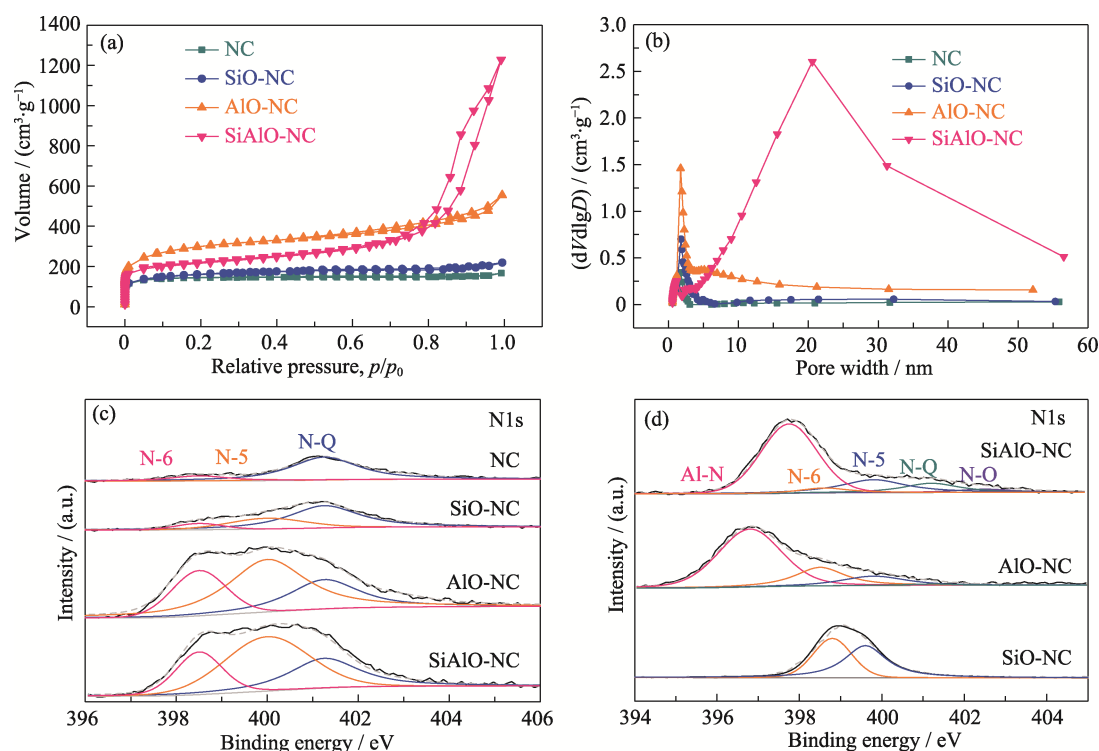
Fig. 3　(a) Nitrogen adsorption-desorption isotherms and (b) pore size distributions of NC, SiO-NC, AlO-NC, SiAlO-NC
(after removing templates), N1s XPS spectra of (c) NC, SiO-NC, AlO-NC, SiAlO-NC (after removing templates) and
(d) SiO-NC, AlO-NC, SiAlO-NC (without removing templates)

Table 1　BET and elemental parameters of samples

Sample	SSA /(m²·g⁻¹)	Pores volume /(cm³·g⁻¹)	N /at%	N-6 /at%	N-5 /at%
NC	440.78	0.07	1.42	0.21	0.03
SiO-NC	520.78	0.19	1.66	0.14	0.44
AlO-NC	980.35	0.68	3.52	0.78	1.75
SiAlO-NC	703.20	1.78	5.29	1.17	2.53

Firstly, previous studies suggest that the high surface area with more defects and edges in the carbon materials facilitates the formation of the high nitrogen and active nitrogen contents[17]. Therefore, considering that AlO-NC has more defects than SiO-NC and NC, the nitrogen content of AlO-NC should be higher than those of SiO-NC and NC, in accordance with the result of XPS spectra.

Although the specific surface area and defects of SiAlO-NC are less than those of AlO-NC, the nitrogen content of SiAlO-NC (5.29at%) is higher than that of AlO-NC (3.52at%). Thus, to further explore the mechanism, we deconvolute N1s band of SiO-NC, AlO-NC and SiAlO-NC without removing templates (Fig. 3(d)). The Al–N bonding forms in AlO-NC and SiAlO-NC. The peak position (binding energy) of the Al–N bonding in SiAlO-NC is higher than that in AlO-NC, suggesting the interaction between Si–O–Si network and Al–N. This interaction could promote the activity of oxygen atoms in oxides because SiAlO-NC owns relatively strong N–O bonding in contrast with SiO-NC and AlO-NC. After etching, nearly no N–O bonding exists in SiAlO-NC, SiO-NC and AlO-NC, so that oxygen atoms in oxides bond with nitrogen atoms in carbon materials for SiAlO-NC in the sintering process, making the nitrogen atoms difficult to escape.

Besides, the N1s bands of the carbon materials, which are prepared at 900 and 1100 ℃ for SiAlO-NC, are also deconvoluted, as shown in Fig. S3 and Table S1. Clearly, the interaction between Si–O–Si network and Al–N bonding is independent of the sintering temperature for carbon materials, which suggests that this method is promising for tuning nitrogen species and content in carbon materials, achieving high active N content for electrochemical fields, such as supercapacitors and electrocatalysis.

To explore the importance of tuning N species and content in these carbon materials, three-electrode electrochemical cells are assembled in aqueous solution. Considering that the prepared carbon materials have the best electrochemical performances in 1.0 mol·L⁻¹ H_2SO_4, it is chosen as aqueous solution electrolyte. Cyclic voltammetry (CV) curves at 10 mV·s⁻¹ (Fig. 4(a)) are approximately rectangular, even at 100 mV·s⁻¹ (Fig. S4(a)). These results show that the prepared carbon materials own good capacitive behavior. For SiAlO-NC, two Faradaic

peaks (one during charging, another during discharging) are almost symmetric and obvious in Fig. 4(a), owing to the high active N content. With the introduction of oxides, the capacitance is gradually improved due to higher specific surface area and active N content. Specifically, SiAlO-NC has the best performance at all current densities and achieves 302 $F \cdot g^{-1}$ at 1 $A \cdot g^{-1}$, which is higher than those of NC (160 $F \cdot g^{-1}$), SiO-NC (180 $F \cdot g^{-1}$) and AlO-NC (240 $F \cdot g^{-1}$) (Fig. 4(b) and Fig. S5). To find the optimal nitrogen-rich carbon material, we tried different heating temperatures, and SiAlO-NC at 1000 ℃ still shows the best performance (Fig. S6). SiAlO-NC achieves 218 $F \cdot g^{-1}$ at the current density of 20 $A \cdot g^{-1}$ and 177 $F \cdot g^{-1}$ at 120 $A \cdot g^{-1}$ (Fig. S4(b)). The cycling stability of SiAlO-NC is extraordinary at 20 $mV \cdot s^{-1}$. After 20000 cycles, the capacitive retention is about 92% in 1 $mol \cdot L^{-1}$ H_2SO_4 (Fig. S7). The excellent capacitive performance origins from the high-temperature sintering process, leading to the interaction between Si–O–Si network and aluminum oxide, thereby empowering high electronic conductivity, active nitrogen content, hierarchical pore structure and 3D interconnected structure in SiAlO-NC.

We assembled two-electrode electrochemical cells, using symmetric SiAlO-NC electrodes, and tested at operating voltage (1.2 V) in aqueous solution (1.0 $mol \cdot L^{-1}$ H_2SO_4) for validating electrochemical performance. CV curves at 10 $mV \cdot s^{-1}$ are nearly rectangular (Fig. 4(c)),

even at 100 $mV \cdot s^{-1}$ (Fig. S8). GCD curves (Fig. S9(a)), even at 40 $A \cdot g^{-1}$ (Fig. S9(b)), are almost linear and symmetrical. All these results reflect the purely capacitive behavior of SiAlO-NC. Ragone plots for SiAlO-NC and other reported nitrogen-carbon materials are shown in Fig. 4(d). At 300 $W \cdot kg^{-1}$, the energy density of SiAlO-NC is calculated to be 13.41 $Wh \cdot kg^{-1}$, which is higher than those of most reported nitrogen-carbon materials[18-23], indicating that it is a comparable electrode material for supercapacitors (Table S2).

3 Conclusions

In summary, we successfully tuned nitrogen species and content by the interaction between Si–O–Si network and aluminum oxide. Different morphology designs also affect the defect concentration, specific surface area, pore size distribution and pore volume. This interaction between Si–O–Si network and Al–N affects the activities of oxygen atoms in oxides, which provides oxygen-induced nitrogen fixation. As-prepared N-rich carbon material is endowed with high nitrogen doping level of 5.29at%, high pore volume of 1.78 $cm^3 \cdot g^{-1}$, hierarchical pore structure of 0.5–60 nm, and 3D interconnected structure. Therefore, these synergetic effects give rise to high capacitance of 302 $F \cdot g^{-1}$, excellent rate capability of 177 $F \cdot g^{-1}$ at 120 $A \cdot g^{-1}$ and good durability (92% after
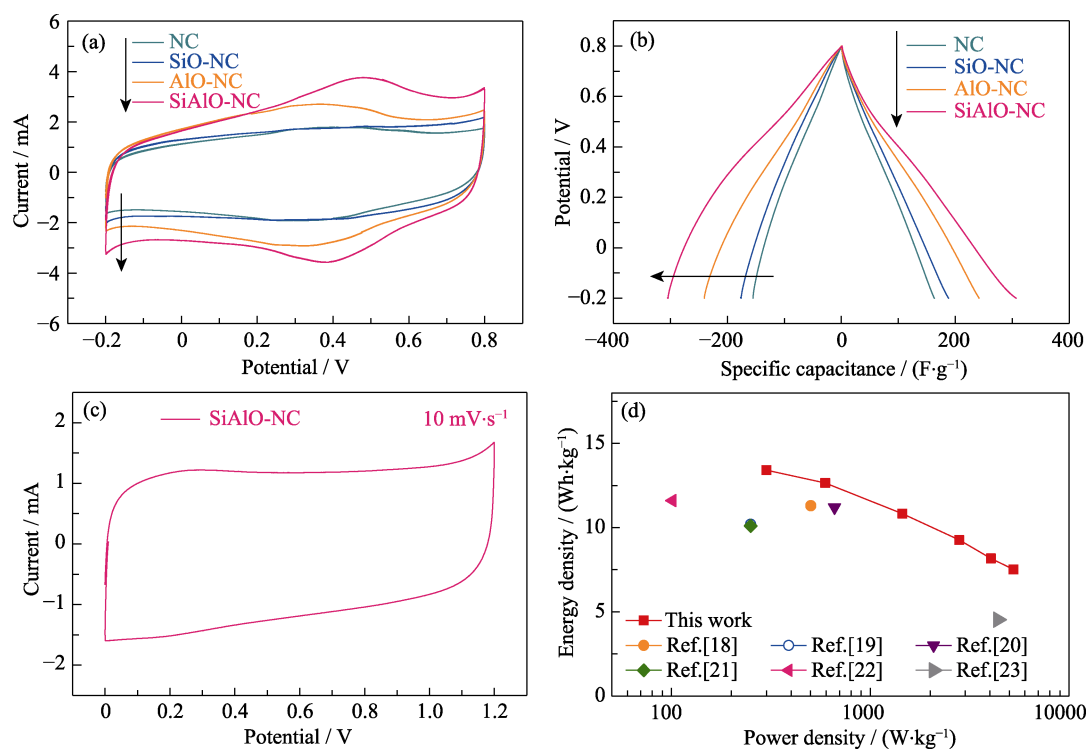

Fig. 4 (a) CV curves at 10 $mV \cdot s^{-1}$ and (b) galvanostatic charge/discharge (GCD) curves of NC, SiO-NC, AlO-NC, SiAlO-NC at 1 $A \cdot g^{-1}$ in three-electrode configuration; (c) CV curve of symmetric cell with SiAlO-NC, and (d) Ragone plots for SiAlO-NC and other nitrogen-carbon materials

20 000 cycles). This strategy to tune nitrogen species and content in carbon materials at high temperature is a promising method to prepare high performance N-rich carbon materials.

Supporting materials

Supporting materials related to this article can be found at https://doi.org/10.15541/jim20200498.

References:

[1] ZHANG L L, ZHAO X S. Carbon-based materials as supercapacitor electrodes. *Chemical Society Reviews*, 2009, **38:** 2520–2531.

[2] HAO Y X, QIAN M, XU J J, *et al*. Porous cotton-derived carbon: synthesis, microstructure and supercapacitive performance. *Journal of Inorganic Materials*, 2018, **33(1):** 93–99.

[3] YU J H, XU L L, ZHU Q Q, *et al*. Superior electrochemical performance of graphene *via* carboxyl functionalization and surfactant intercalation. *Journal of Inorganic Materials*, 2016, **31(2):** 220–224.

[4] HWANG J Y, LI M P, EI-KADY M F, *et al*. Next-generation activated carbon supercapacitors: a simple step in electrode processing leads to remarkable gains in energy density. *Advanced Functional Materials*, 2017, **27:** 1605745.

[5] ZHOU Y, JIA Z X, SHI L L, *et al*. Pressure difference-induced synthesis of P-doped carbon nanobowls for high-performance supercapacitors. *Chemical Engineering Journal*, 2020, **385:** 123858.

[6] SEREDYCH M, HULICOVA-JURCAKOVA D, LU G Q, *et al*. Surface functional groups of carbons and the effects of their chemical character, density and accessibility to ions on electrochemical performance. *Carbon*, 2008, **46:** 1475–1488.

[7] HAN S W, BANG J, KO S H, *et al*. Variation of nitrogen species in zeolite-templated carbon by low-temperature carbonization of pyrrole and the effect on oxygen reduction activity. *Journal of Materials Chemistry A*, 2019, **7:** 8353–8360.

[8] LI S Y, GU Q Q, CAO N, *et al*. Defect enriched N-doped carbon nanoflakes as robust carbocatalysts for H_2S selective oxidation. *Journal of Materials Chemistry A*, 2020, **8:** 8892–8902.

[9] CHOI C H, PARK S H, WOO S I. Binary and ternary doping of nitrogen, boron, and phosphorus into carbon for enhancing electrochemical oxygen reduction activity. *ACS Nano*, 2012, **6(8):** 7084–7091.

[10] HE H, HUANG D, TANG Y G, *et al*. Tuning nitrogen species in three-dimensional porous carbon *via* phosphorus doping for ultra-fast potassium storage. *Nano Energy*, 2019, **57:** 728–736.

[11] TO J W F, HE J J, MEI J G, *et al*. Hierarchical N-doped carbon as CO_2 adsorbent with high CO_2 selectivity from rationally designed polypyrrole precursor. *Journal of The American Chemical Society*, 2016, **138(3):** 1001–1009.

[12] SU F B, TIAN Z Q, POH C K, *et al*. Pt nanoparticles supported on nitrogen-doped porous carbon nanospheres as an electrocatalyst for fuel cells. *Chemistry of Materials*, 2010, **22:** 832–839.

[13] LIU R L, SHI Y F, WAN Y, *et al*. Triconstituent co-assembly to ordered mesostructured polymer-silica and carbon-silica nanocomposites and large-pore mesoporous carbons with high surface areas. *Journal of The American Chemical Society*, 2006, **128:** 11652–11662.

[14] FERRARI A C, ROBERTSON J. Interpretation of Raman spectra of disordered and amorphous carbon. *Physical Review B*, 2000, **61(20):** 14095–14107.

[15] XU F, SUN P, QIAN M, *et al*. Variable texture few-layer ordered macroporous carbon for high-performance electrochemical capacitors. *Journal of Materials Chemistry A*, 2017, **5:** 25171–25176.

[16] WANG H B, MAIYALAGAN T, WANG X. Review on recent progress in nitrogen-doped graphene: synthesis, characterization, and its potential applications. *ACS Catalysis*, 2012, **2(5):** 781–794.

[17] SUN J, WANG L, SONG R, *et al*. Enhancing pyridinic nitrogen level in graphene to promote electrocatalytic activity for oxygen reduction reaction. *Nanotechnology*, 2016, **27:** 055404.

[18] SUN H, QUAN H Y, PAN M H, *et al*. Nitrogen-doped hierarchically structured porous carbon as a bifunctional electrode material for oxygen reduction and supercapacitor. *Journal of Alloys and Compounds*, 2020, **826:** 154208.

[19] DEKA N, BARMAN J, KASTHURI S, *et al*. Transforming waste polystyrene foam into N-doped porous carbon for capacitive energy storage and deionization applications. *Applied Surface Science*, 2020, **511:** 145576.

[20] DU J, CHEN A B, LIU L, *et al*. N-doped hollow mesoporous carbon spheres prepared by polybenzoxazines precursor for energy storage. *Carbon*, 2020, **160:** 265–272.

[21] WANG Y Z, LIU Y X, WANG D H, *et al*. Free-standing honeycomb-like N doped carbon foam derived from coal tar pitch for high-performance supercapacitor. *Applied Surface Science*, 2020, **506:** 145014.

[22] HUO S L, ZHANG X L, LIANG B L, *et al*. Synthesis of interconnected hierarchically porous carbon networks with excellent diffusion ability based on $NaNO_3$ crystal-assisted strategy for high performance supercapacitors. *Journal of Power Sources*, 2020, **450:** 227612.

[23] YUKSEL R, BUYUKCAKIR O, PANDA P K, *et al*. Necklace-like nitrogen doped tubular carbon 3D frameworks for electrochemical energy storage. *Advanced Functional Materials*, 2020, **30(10):** 1909725.

基于结构调节碳材料的掺氮种类和含量及其
超级电容器储能应用

孙　鹏[1,2], 张绍宁[1,3], 毕　辉[1], 董武杰[1], 黄富强[1,3,4]

(1. 中国科学院 上海硅酸盐研究所, 高性能陶瓷和超微结构国家重点实验室, 上海 200050; 2. 中国科学院大学 材料科学与光电技术学院, 北京 100049; 3. 上海科技大学 物理科学与技术学院, 上海 200031; 4. 北京大学 化学与分子工程学院, 稀土材料化学及应用国家重点实验室, 北京 100871)

摘　要: 碳材料是极具潜力的超级电容器电极材料, 但是其容量较低。异质原子掺杂, 尤其是氮掺杂, 是大幅度提高碳材料电化学性能的有效方法。但是在碳材料中实现高含量的活性氮掺杂仍极具挑战。本研究通过 Si–O–Si 网络和氧化铝之间的相互作用成功调节碳材料的掺氮种类及其含量。除此之外, 通过调节前驱体组成, 碳材料的结构可以从珊瑚状转变为三维结构。在反应中, 氧化物中的氧原子可以和碳材料中氮原子成键, 氮原子不易逃离, 从而实现高含量氮掺杂(5.29at%@1000 ℃)。另一方面, 相互作用使碳材料孔体积增大(1.78 $m^3 \cdot g^{-1}$)和孔径分布加宽(0.5~60 nm)。因此, 获得的富氮掺杂碳材料具有 302 $F \cdot g^{-1}$@1 $A \cdot g^{-1}$ 的高容量和 177 $F \cdot g^{-1}$@120 $A \cdot g^{-1}$ 的杰出倍率性能。此独特的固氮方法是一种有潜力的制备高性能超级电容器电极材料的策略。

关　键　词: 碳材料; 氮原子固定; 相互作用; 形貌设计; 超级电容器

中图分类号: O782　　**文献标志码:** A

Supporting materials:

Tuning Nitrogen Species and Content in Carbon Materials through Constructing Variable Structures for Supercapacitors

SUN Peng[1,2], ZHANG Shaoning[1,3], BI Hui[1], DONG Wujie[1], HUANG Fuqiang[1,3,4]

(1. State Key Laboratory of High Performance Ceramics and Superfine Microstructure, Shanghai Institute of Ceramics, Chinese Academy of Sciences, Shanghai 200050, China; 2. Center of Materials Science and Optoelectronics Engineering, University of Chinese Academy of Sciences, Beijing 100049, China; 3. School of Physical Science and Technology, ShanghaiTech University, Shanghai 200031, China; 4. State Key Laboratory of Rare Earth Materials Chemistry and Applications, College of Chemistry and Molecular Engineering, Peking University, Beijing 100871, China)

Electrochemical characterization

To fabricate supercapacitor electrodes, 20 mg of the active material and 10 mg of poly(vinylidene fluoride) PVDF were mixed in 2 mL of *N*-methyl-2-pyrrolidone. Then 100 μL slurry was coated onto a graphene foam, which was used as the collector. The electrode had exposed surface area of 1 cm×1 cm and was dried at 120 ℃ under vacuum. Electrochemical tests were performed on a CHI 760E electrochemical workstation (Shanghai Chenhua).

Results and discussion

There are some similarities among as-prepared carbon materials. In Raman spectra (Fig. S1(a)), there is a weak signal of 2D in all carbon materials, which suggests that they are composed of crystalline carbon, identical with the observation in XRD (Fig. S1(b)). Two broad peaks in all samples at about 24.0° and 43.5° correspond to the (002) and (101) crystal planes of the graphite structure. However, the broad peaks at about 24.0° are slightly shifted to the left compared to graphite, which suggests that the interlayer distance, *d*-spacing, increases through this method.

Resistances of devices can be evaluated by electrochemical impedance spectroscopy (EIS) (Fig. S10), which is presented in Nyquist plots, fitting with the equivalent Randles circuit. According to the Nyquist plots, R_b (Ohmic resistance) is 1.62 Ω for NC, 1.56 Ω for SiO-NC, 1.59 Ω for AlO-NC and 1.44 Ω for SiAlO-NC, suggesting the resistance for SiAlO-NC is the lowest. This low resistance probably results from the wetting of materials improved by nitrogen doping, which lowers the interface resistance. R_{ct} (charge-transfer resistance) is 0.44 Ω for NC and 0.40 Ω for SiAlO-NC, which suggests that the charge-transfer kinetic improves with the interaction between Si–O–Si network and aluminum oxide. The absence of a semicircle at high frequencies

for all four kinds of materials likely signifies fast ion diffusion in the electrodes. The impedance plots for NC, SiO-NC, AlO-NC and SiAlO-NC are all parallel to
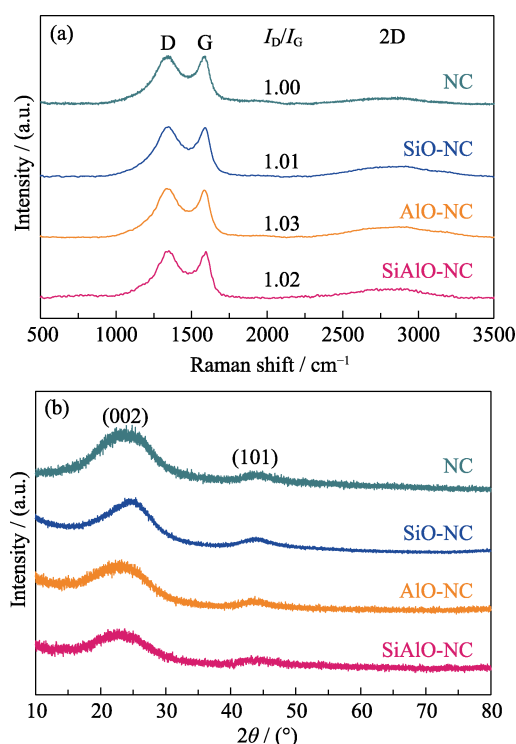

Fig. S1   (a) Raman spectra and (b) XRD patterns of NC, SiO-NC, AlO-NC and SiAlO-NC
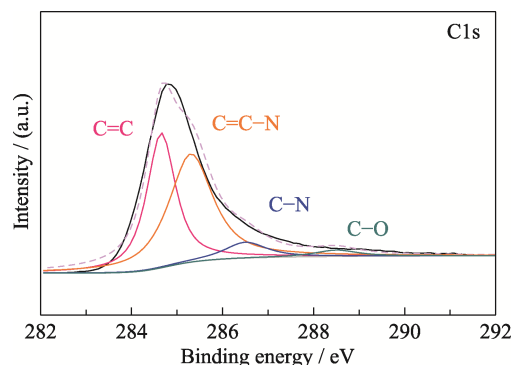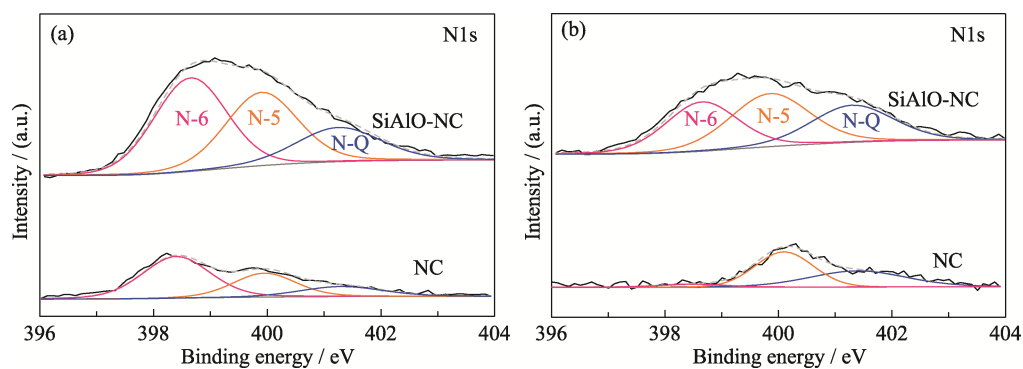

Fig. S2   C1s XPS spectrum of SiAlO-NC

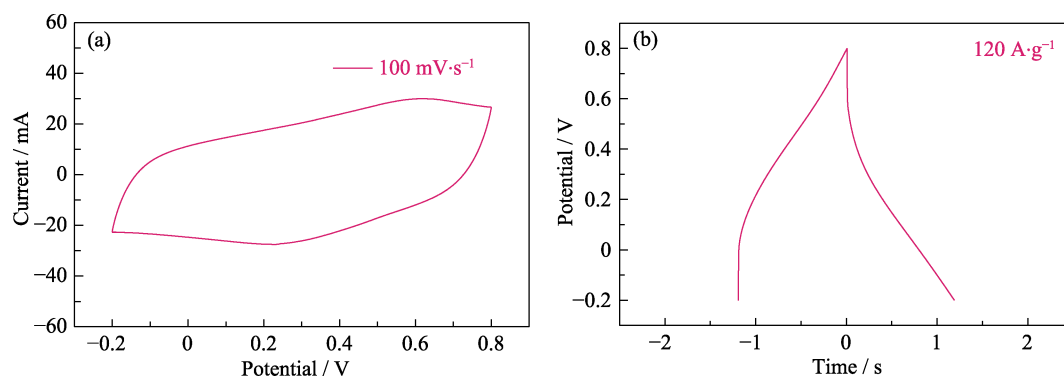Fig. S3　N1s XPS spectra of NC and SiAlO-NC at (a) 900 and (b) 1100 ℃

Fig. S4　(a) CV curve at 100 mV·s⁻¹ and (b) GCD curve at 120 A·g⁻¹ of SiAlO-NC in three-electrode configuration
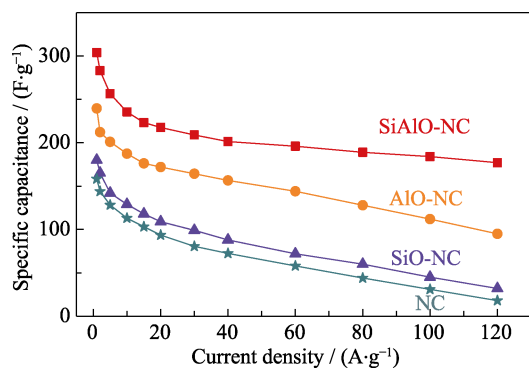

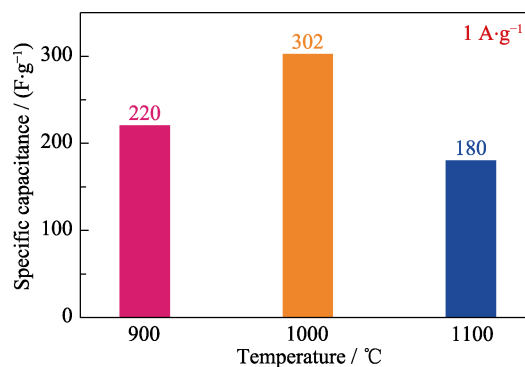Fig. S5　Specific capacitances calculated from GCD curves *vs.* current density for NC, SiO-NC, AlO-NC and SiAlO-NC

Fig. S6　Histograms of specific capacitance for SiAlO-NC at 1 A·g⁻¹ *vs.* the heating temperature
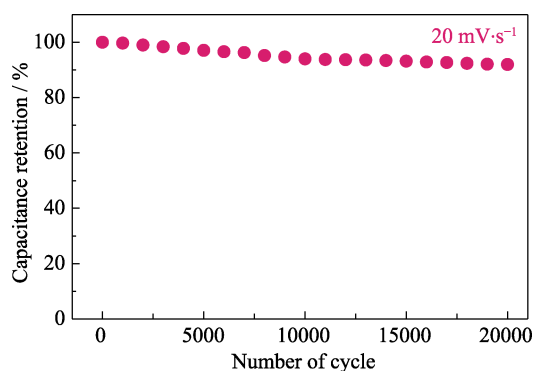

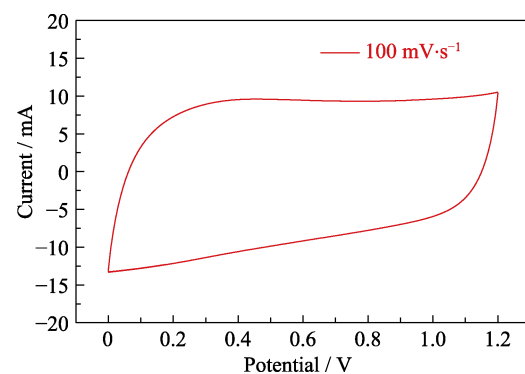Fig. S7　Cycling performance of SiAlO-NC electrode measured in three-electrode configuration

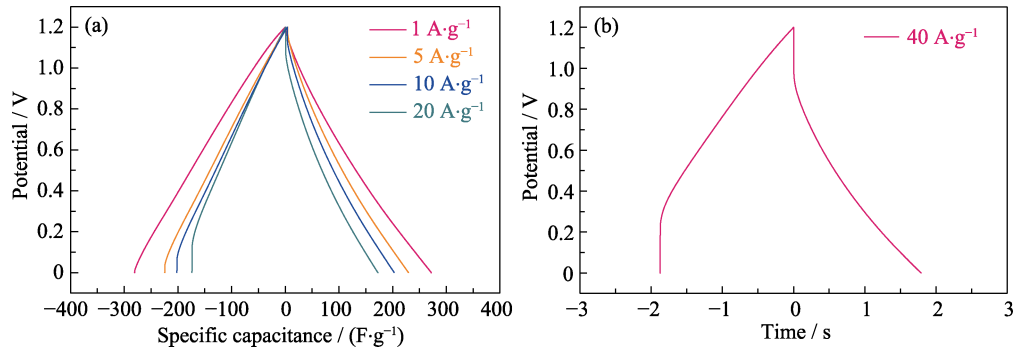Fig. S8　CV curve of SiAlO-NC electrode measured in symmetric electrochemical cell at 100 mV·s⁻¹

Fig. S9　GCD curves of SiAlO-NC electrode measured in symmetric electrochemical cells at
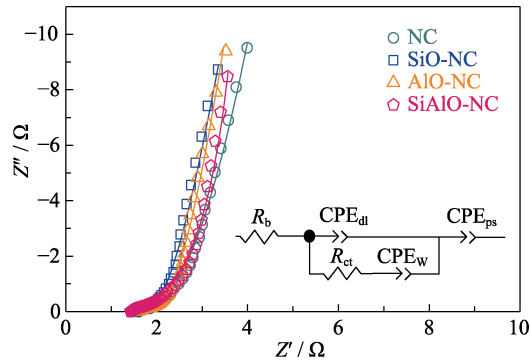(a) different current densities and (b) 40 A·g^{-1}

Fig. S10　Nyquist plots over 0.01 to 10^5 Hz of NC, SiO-NC, AlO-NC and SiAlO-NC based on the fittings using equivalent Randles circuit model(inset) in three-electrode configuration

Electrochemical analysis

To further explore components of the capacitance in SiAlO-NC, the total capacitance is divided into two parts, which are rate-independent (such as EDLC) and diffusion-limited component (such as intercalation), according to the equation[1]:

$$C = k_1 + k_2 v^{-1/2} \qquad (S1)$$

Here, on the right-hand side, $k_2 v^{-1/2}$ is the diffusion-limited component. The potential scan rate, v, is inversely proportional to the half-cycle time (T) in CV and CC tests. In CV test, T is the time required to sweep over the voltage window. In the CC test, it is the time required to discharge. The rate-independent part, k_1, dominates in SiAlO-NC at about 235 F·g^{-1}, from Fig. S11(a). The high k_1 suggests that SiAlO-NC owns good rate capability

vertical lines at low frequencies, indicating the pure capacitive behavior.
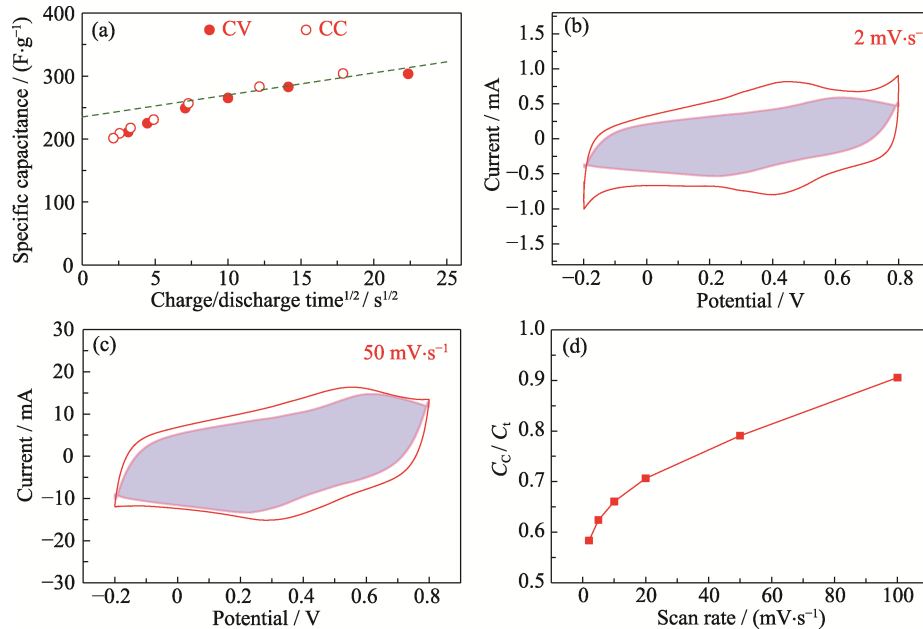
Fig. S11　Electrochemical performance of the SiAlO-NC sample

(a) Capacitance *versus* discharge time, $t^{1/2}$. Hollow symbols: CC test data, solid symbols: CV test data from 2 to 100 mV·s^{-1};
Extrapolation of capacitance to t=0 gives a rate-independent capacitance; Instantaneous current of the SiAlO-NC sample at
(b) 2 and (c) 50 mV·s^{-1}, giving the shaded loop is the capacitive capacitance, and the region outside is the pseudocapacitance;
(d) Fraction of capacitive capacitance C_c in total capacitance C_t

Table S1　Characteristic summary of NC and SiAlO-NC

Sample	N/at%	N-6/at%	N-5/at%	N-Q/at%	Sample	N/at%	N-6/at%	N-5/at%	N-Q/at%
NC (900 ℃)	2.81	1.54	0.82	0.45	NC (1100 ℃)	0.61	0.03	0.32	0.26
SiAlO-NC (900 ℃)	8.27	3.65	3.00	1.62	SiAlO-NC (1100 ℃)	4.33	1.61	1.27	1.45

Table S2 Comparison of the specific capacitances, rate capabilities and cycling performances for previously reported N-doped porous carbon materials

Carbon material	Specific capacitance /(F·g^{-1})	Rate capability /(F·g^{-1})	Cycling performance	Ref.
N-doped porous carbon	327 at 1 A·g^{-1}	200 at 20 A·g^{-1}	10000 cycles@100%	[2]
N/S co-doped porous carbon	272 at 1 A·g^{-1}	172 at 100 A·g^{-1}	5000 cycles at 5 A·g^{-1}@97.1%	[3]
N/O co-doped carbon	242 at 0.5 A·g^{-1}	132 at 20 A·g^{-1}	10000 cycles at 5 A·g^{-1}@97%	[4]
Graphene/N-rich carbon	229 at 1 A·g^{-1}	196 at 10 A·g^{-1}	10000 cycles at 2 A·g^{-1}@99.5%	[5]
N-doped carbon foam	280 at 1 A·g^{-1}	185 at 40 A·g^{-1}	10000 cycles at 5 A·g^{-1}@96.3%	[6]
N-doped tubular carbon	204 at 0.1 A·g^{-1}	173 at 10 A·g^{-1}	50000 cycles at 5 A·g^{-1}@91.5%	[7]
N-doped carbon microtube	309 at 1 A·g^{-1}	220 at 10 A·g^{-1}	10000 cycles at 1 A·g^{-1}@94%	[8]
N-doped porous carbon	292 at 1 A·g^{-1}	200 at 20 A·g^{-1}	10000 cycles at 1 A·g^{-1}@86%	[9]
N-doped carbon nanorod	271 at 0.5 A·g^{-1}	175 at 20 A·g^{-1}	10000 cycles at 5 A·g^{-1}@97%	[10]
3D porous carbon	261 at 0.5 A·g^{-1}	200 at 10 A·g^{-1}	5000 cycles at 1 A·g^{-1}@96%	[11]
N-doped porous carbon	250 at 1.0 A·g^{-1}	160 at 10 A·g^{-1}	3000 cycles at 1 A·g^{-1}@97.3%	[12]
N-doped carbon spheres	301 at 0.2 A·g^{-1}	210 at 5 A·g^{-1}	5000 cycles at 5 A·g^{-1}@100%	[13]
N-doped porous carbon	252 at 1.0 A·g^{-1}	189 at 15 A·g^{-1}	10000 cycles at 15 A·g^{-1}@94%	[14]
N-doped porous carbon	334 at 1.0 A·g^{-1}	215 at 20 A·g^{-1}	10000 cycles at 20 mV·s^{-1}@95.2%	[15]
3D graphene-like carbon	252 at 1.0 A·g^{-1}	168 at 50 A·g^{-1}	5000 cycles at 50 mV·s^{-1}@98%	[16]
SiAlO-NC	302 at 1 A·g^{-1}	218 at 20 A·g^{-1} 177 at 120 A·g^{-1}	20000 cycles at 20 mV·s^{-1}@92%	This work

and high double-layer capacitance, owing to the high-temperature sintering process and the interaction between Si–O–Si network and aluminum oxide. On one hand, SiAlO-NC is prepared at high temperature (1000 ℃), which results in high electronic conductivity in the carbon material. On the other hand, the interaction between Si–O–Si network and aluminum oxide leads to high pore volume (1.78 cm^3·g^{-1}), the hierarchical pore structure (0.5–60 nm) and 3D interconnected structure in SiAlO-NC, which is convenient for ions in the electrolyte to approach the active sites in the carbon material. The other part of the capacitance, $k_2 v^{-1/2}$, originating from the pseudocapacitance is ~70 F·g^{-1}. Thus, this material shows the combination of pseudocapacitance and electric double-layer capacitance.

The currents at each potential are deconvoluted into currents proportional to v and $v^{1/2}$ in the CV curves. The former is a capacitive CV loop, as shown in Fig. S11(b-c)[1]. Here, the shaded loop represents the capacitor-like charge storage. The fraction of capacitive capacitance C_c in the total capacitance C_t is calculated

according to the shaded loop (Fig. S11(d)).

References:

[1] LIN T Q, CHEN I W, LIU F X, et al. Nitrogen-doped mesoporous carbon of extraordinary capacitance for electrochemical energy storage. *Science*, 2015, **350**: 1508–1513.

[2] DEKA N, BARMAN J, KASTHURI S, et al. Transforming waste polystyrene foam into N-doped porous carbon for capacitive energy storage and deionization applications. *Appl. Surf. Sci.*, 2020, **511**: 145576.

[3] HUO S, LIU M, WU L, et al. Methanesulfonic acid-assisted synthesis of N/S co-doped hierarchically porous carbon for high performance supercapacitors. *J. Power Sources*, 2018, **387**: 81–90.

[4] ZHANG R, JING X, CHU Y, et al. Nitrogen/oxygen co-doped monolithic carbon electrodes derived from melamine foam for high-performance supercapacitors. *J. Mater. Chem. A*, 2018, **6**: 17730–17739.

[5] CHEN Y, XIAO Z, LIU Y, et al. A simple strategy toward hierarchically porous graphene/nitrogen-rich carbon foams for high-performance supercapacitors. *J. Mater. Chem. A*, 2017, **5**: 24178–24184.

[6] WANG Y, LIU Y, WANG D, et al. Free-standing honeycomb-like N doped carbon foam derived from coal tar pitch for high-performance supercapacitor. *Appl. Surf. Sci.*, 2020, **506**: 145014.

[7] YUKSEL R, BUYUKCAKIR O, PANDA P K, *et al*. Necklace-like nitrogen doped tubular carbon 3D frameworks for electrochemical energy storage. *Adv. Funct. Mater.*, 2020, **30:** 1909725.

[8] LUO J D, ZHANG H, ZAHNG Z, *et al*. In-built template synthesis of hierarchical porous carbon microcubes from biomass toward electrochemical energy storage. *Carbon*, 2019, **155:** 1–8.

[9] ZHU D, JIANG J, SUN D, *et al*. A general strategy to synthesize high-level N-doped porous carbons *via* schiff-base chemistry for supercapacitors. *J. Mater. Chem. A*, 2018, **6:** 12334–12343.

[10] ZHENG L P, TANG B, DAI X C, *et al*. High-yield synthesis of N-rich polymer-derived porous carbon with nanorod-like structure and ultrahigh N-doped content for high-performance superca-pacitors. *Chemical Engineering Journal*, 2020, **399:** 125671.

[11] TONG X, ZHUO H, WANG S, *et al*. A new strategy to tailor the structure of sustainable 3D hierarchical porous N-self-doped car-bons from renewable biomass for high-performance superca-pacitors and CO_2 capture. *RSC Advances*, 2016, **6:** 34261–34270.

[12] WANG D H, CHEN Y, YANG H Q, *et al*. N-doped porous carbon anchoring on carbon nanotubes derived from ZIF-8/polypyrrole nanotubes for superior supercapacitor electrodes. *Applied Surface Science*, 2018, **457:** 1018–1024.

[13] WANG T, SUN Y, ZHANG L L, *et al*. Space-confined polymerization: controlled fabrication of nitrogen-doped polymer and carbon microspheres with refined hierarchical architectures. *Advanced Materials*, 2019, **31:** 1807876.

[14] HAO Y X, QIAN M, XU J J, *et al*. Porous cotton-derived carbon: synthesis, microstructure and supercapacitive performance. *Journal of Inorganic Materials*, 2018, **33(1):** 93–99.

[15] QIAN M, WANG Z M, LI Z, *et al*. Sol–gel assisted chemical activation for nitrogen doped porous carbon. *Microporous Mesoporous Materials*, 2019, **286:** 18–24.

[16] XU F, LIN T Q, BI H, *et al*. Graphene-like carbon with three-dimensional periodicity prepared from organic-inorganic templates for energy storage application. *Carbon*, 2017, **111:** 128–132.